Rapid Communications

Ordered structure of $FeGe_2$ formed during solid-phase epitaxy

B. Jenichen,* M. Hanke, S. Gaucher, A. Trampert, and J. Herfort
Paul-Drude-Institut für Festkörperelektronik, Leibniz-Institut im Forschungsverbund Berlin e.V., Hausvogteiplatz 5–7, D-10117 Berlin, Germany

H. Kirmse and B. Haas
Humboldt-Universität zu Berlin, Institut für Physik, Newtonstraße 15, D-12489 Berlin, Germany

E. Willinger and X. Huang
Fritz-Haber-Institut der Max-Planck-Gesellschaft, Faradayweg 4, D-14195 Berlin, Germany

S. C. Erwin
Center for Computational Materials Science, Naval Research Laboratory, Washington, DC 20375, USA

(Received 11 April 2018; published 21 May 2018)

$Fe_3Si/Ge(Fe,Si)/Fe_3Si$ thin-film stacks were grown by a combination of molecular beam epitaxy and solid-phase epitaxy (Ge on Fe_3Si). The stacks were analyzed using electron microscopy, electron diffraction, and synchrotron x-ray diffraction. The Ge(Fe,Si) films crystallize in the well-oriented, layered tetragonal structure $FeGe_2$ with space group $P4mm$. This kind of structure does not exist as a bulk material and is stabilized by the solid-phase epitaxy of Ge on Fe_3Si. We interpret this as an ordering phenomenon induced by minimization of the elastic energy of the epitaxial film.

DOI: 10.1103/PhysRevMaterials.2.051402

Ordering phenomena of epitaxial layers have been found in semiconductor mixed crystals as well as in metallic alloys. In general, the ordering has a strong influence on the physical properties of the epitaxial films. In semiconductors (SCs), the formation of monolayer superlattices in mixed crystal $Al_xGa_{1-x}As$ epitaxial films grown by metal-organic chemical vapor deposition on (110)- or (100)-oriented GaAs substrates has been observed [1]. The authors suggested that this long-range ordering is a thermodynamically stable phase at temperatures below about 800 °C. A strain-induced order-disorder transition was found in SiGe epitaxial films grown on Si(001) by molecular beam epitaxy (MBE) [2]. This phenomenon later was explained using self-consistent total energy calculations [3,4].

For metallic alloys, the amount of collected data is even larger [5–11]. Here, the influence of ordering on material properties such as hardness, conductivity, magnetism, and corrosion resistance is important. The elastic interaction of the different atoms of the alloys often leads to energetically favored ordered structures. This kind of ordering is influenced by the anisotropy of the crystal lattice.

The structures of the epitaxial Ge and Fe_3Si films on GaAs substrates correspond well to the known structures of their bulk materials [12–14]. However, when the Fe_3Si film is used as a substrate for epitaxial growth of Ge, the influence of the Fe_3Si structure on the growing epitaxial Ge film unexpectedly turns out to be stronger and ordering phenomena occur. These ordering phenomena are induced by the epitaxial growth and were not observed in bulk materials up to now. Several methods were applied to achieve perfect semiconducting Ge films on top of ferromagnetic (FM) layers [15–17]. Recently, the method of the solid-phase epitaxy (SPE) of Ge was utilized in order to achieve a perfect crystallinity of the film and superior interface quality [18–20]. However, the diffusion of Fe and Si was not entirely prevented during the annealing process. Therefore, the Ge film contained some amount of Fe and Si, leading to a shift of the x-ray diffraction (XRD) peak of the Ge(Fe,Si) film and the formation of a superlatticelike structure inside the Ge(Fe,Si) film. The FM Fe_3Si forms Schottky contacts with the SC Ge and GaAs [21]. A triple-layer structure FM-SC-FM is therefore suitable for Schottky barrier tunneling transistors described in Ref. [22], similar to tunneling magnetoresistance devices [23,24]. A spin-dependent transport of holes was detected up to room temperature [20]. The aim of the present Rapid Communication is the investigation of the structure of the Ge(Fe,Si) film.

$Fe_3Si/Ge(Fe,Si)/Fe_3Si$ thin-film stacks were grown combining MBE for Fe_3Si on GaAs(001) and SPE for Ge on Fe_3Si [18]. A 36-nm-thick Fe_3Si film was grown by MBE on the GaAs buffer layer at a growth rate of 16 nm/h and a temperature of 200 °C in a separate growth chamber dedicated to metal growth. In the same chamber the 4-nm-thick Ge film was deposited at 150 °C, resulting in a smooth interface but with an amorphous structure. For the SPE of the Ge film the sample was heated at 5 K/min up to a temperature of 240 °C and then annealed for 10 min. The 12-nm-thick upper Fe_3Si film was then grown by MBE on top of the crystalline Ge under the same conditions as the lower Fe_3Si film. The growth and annealing conditions of the sample result

*bernd.jenichen@pdi-berlin.de

 ©2018 American Physical Society

in a typical structure characteristic for the whole series [18]. After sample preparation, transmission electron microscopy (TEM) and XRD (here at an energy of $E = 10$ keV) were used for structural characterization. Experimental details are given in the Supplemental Material [25]. TEM and XRD simulations were performed using available software packages [26–28]. In addition, density functional theory (DFT) was employed for the calculation of the lattice parameter and the electronic band structure of the Ge(Fe,Si). DFT in the generalized gradient approximation [29] was applied using the Vienna *ab initio* simulation package [30,31]. The Perdew-Burke-Ernzerhof (PBE) [32] and the Heyd-Scuseria-Ernzerhof (HSE) [33] exchange-correlation functionals were used for the calculations.

From earlier x-ray results it is clear that the diffusion inside the layer stack has an obvious influence on the formation of the structure of the Ge(Fe,Si) film [18]. Here, the diffusion during SPE is more important than the diffusion during the subsequent epitaxial growth of Fe_3Si, because the characteristic structure was observed even without the uppermost Fe_3Si film, and the diffusion during Fe_3Si film growth is known to be low [34]. We obtained the depth dependence of the atomic composition of the different elements by energy dispersive x-ray (EDX) spectroscopy in the scanning TEM (STEM) [25]. The Ge(Fe,Si) film consisted of a Ge content of 60 ± 5 at. %, an Fe content of 35 ± 5 at. %, and a Si content of 5 ± 5 at. % [35]. Considering in a first approximation the binary phase diagram of Fe-Ge, the phases of FeGe and $FeGe_2$ could be expected for the given composition range and an annealing temperature of 240 °C during the SPE process [36]. According to such a consideration the $FeGe_2$ should have the tetragonal Al_2Cu structure ($I4/mcm$) [37].

Let us consider the formation of our Ge(Fe,Si) thin-film structure in more detail. During SPE, an initially amorphous material is annealed on top of a crystalline substrate, resulting in a lattice-matched crystalline epitaxial film. In a solid solution inside the growing film, at first sight a random distribution of the elements on the different lattice sites can be expected. However, an ordered distribution of the solute atoms can sometimes lead to a minimum of the free energy F of the system. The distributions of the different elements can be described in the static concentration-wave formalism [7,8]. A heterogeneity $\Delta(\vec{r})$ can be written as

$$\Delta(\vec{r}) = [n(\vec{r}) - n_0], \tag{1}$$

where $n(\vec{r})$ is the occupation probability of a lattice site with a certain type of atom, n_0 is the average concentration of that element, and $\vec{r}$ is the site vector of the lattice in the crystalline film. The concentration-wave representation of the heterogeneity $\Delta(\vec{r})$ is written as follows: If all the positions of the crystal lattice sites are described by one Bravais lattice, $\Delta(\vec{r})$ can be expanded in a Fourier series, i.e., it can be considered as a superposition of static concentration waves,

$$\Delta(\vec{r}) = \frac{1}{2}\sum_j [Q(\vec{k}_j)\exp(i\vec{k}_j\vec{r}) + Q^*(\vec{k}_j)\exp(-i\vec{k}_j\vec{r})], \tag{2}$$

where $Q(\vec{k}_j)$ is the static concentration-wave amplitude and can be treated as a long-range order parameter, and $\vec{k}_j$ is the nonzero wave vector of the static concentration wave defined in the first Brillouin zone of the disordered alloy. The index j denotes the wave vectors in the Brillouin zone. The ordering can result in a reduction ΔF of the free energy. Then, the uniform solid solution becomes unstable with respect to the heterogeneity (2) with a certain concentration-wave vector $\vec{k} = \vec{k}_0$. In our epitaxial films we clearly observe such an ordering.

In our experiment, the interface between the underlying Fe_3Si film and an amorphous Ge layer is the starting point of the SPE. The lattice mismatch between Ge and Fe_3Si is $\Delta a/a = 1.5 \times 10^{-4}$. During the deposition of the Ge and the subsequent annealing, Fe and Si atoms diffuse into the Ge film, leading to a small but finite lattice mismatch. This lattice mismatch can be compensated not only by a tetragonal distortion of a disordered Ge(Fe,Si) film, but in addition by an ordering of a substitutional solid solution which can be described as a concentration wave with the wave vector $\vec{k}_0$. From symmetry considerations, it is clear that the wave vector of the static concentration wave $\vec{k}_0$ should be perpendicular to the Fe_3Si/Ge(Fe,Si) interface, leaving the properties of the film unchanged along the interface. And indeed, the experimental results obtained earlier by XRD and TEM showed the formation of a superlattice only along one direction, the direction perpendicular to the Fe_3Si/Ge(Fe,Si) interface [18]. A possible choice for the length of the vector is $|\vec{k}_0| = 2\pi/c$, where c is the superstructure period observed. At the same time we take c as the lattice parameter of the growing Ge(Fe,Si) lattice perpendicular to the interface, and a as the lattice parameter parallel to the interface. Such a choice of the lattice leads us to the possibility that the ordering can be described in the frame of the Ge(Fe,Si) lattice itself with a basis of two types of lattice sites described by fractional lattice coordinates: one type occupied mainly by Ge atoms (or Si atoms) and the other mainly by Fe atoms. In this case we can write $(\vec{k}_0 \cdot \vec{r}) = 2\pi z$, where z is the coordinate perpendicular to the Fe_3Si/Ge(Fe,Si) interface. The occupation probability $n(z)$ for a certain type of atom is then

$$n(z) = (1/2)\eta\cos(2\pi z/c) + n_0, \tag{3}$$

where η is the order parameter and n_0 is the average concentration.

A calculation of the change of the free energy ΔF would need more detailed information about the structure of the film. That is why for further investigation of the structure we performed Z-contrast imaging in the STEM. The Z-contrast mode is an incoherent imaging method. In a first approximation presuming constant thickness and neglecting the influence of strain, a high angle annular dark field (HAADF) STEM micrograph exhibits Z contrast: The intensity diffracted by an atomic column is $I_{\mathrm{HAADF}} \sim Z^{1.7\ldots2}$, thus heavier atoms give a brighter image contrast [38]. The intensity increases with the number of atoms in a column as well [39]. The STEM micrographs were evaluated using the method of template matching using the symmetry in the growth plane [40]. Original data are presented in the Supplemental Material [25].

In Fig. 1, we can recognize the superstructure in the Ge-rich Ge(Fe,Si) film. The image of the [100]-oriented sample shows brighter spots forming a square lattice. These spots are caused by Ge columns ($Z = 32$). The darker spots, which occur at the center of every second square, are due to Fe columns ($Z = 26$). In the image of the [110]-oriented sample we see rows of brighter spots and can attribute them to Ge columns.

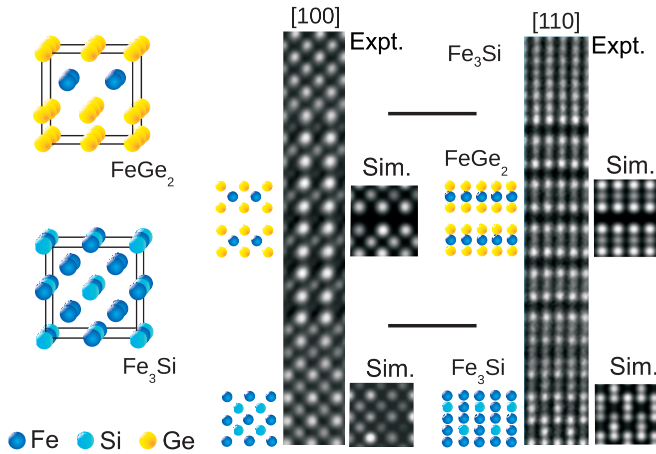

FIG. 1. Comparison of the HAADF experimental cross-section micrographs (larger rectangles, Expt.) with the structural models of $FeGe_2$ $P4mm$ and Fe_3Si shown on the left side as well as the corresponding simulations (small squares, Sim.). The structure of Fe_3Si is well known, whereas the structure of $FeGe_2$ is obtained from the Z contrast of the present micrographs, taken along the two projections [100] and [110]. The horizontal lines mark the positions of the $FeGe_2/Fe_3Si$ interfaces. They are 1 nm long.

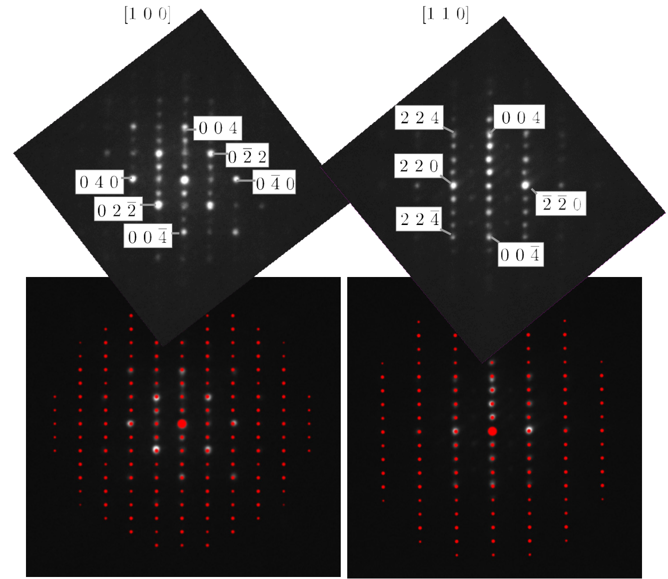

FIG. 2. Nanobeam diffraction patterns of the thin $FeGe_2$ film from [100]-oriented (left) and [110]-oriented (right) samples. The comparison of the experimental patterns with the results of the simulations (red) is given below.

Between every second pair of bright rows we recognize darker spots and consider them as contrasts due to Fe columns. In the Fe_3Si film, we recognize the typical Fe triplets of the image of the [110]-oriented sample and the faint spots of the Si columns between them ($Z = 14$). The image of the [100]-oriented sample shows a square lattice of relatively bright spots with darker spots in the centers of the squares. The DO_3 structure of Fe_3Si corresponding to this kind of contrast is known and can serve as a reference. On the basis of the Z contrast of our HAADF micrographs obtained along the two crystal orientations [100] and [110], we are able to propose a structural model for the Ge(Fe,Si) film: It is the $FeGe_2$ ($P4mm$) structure shown on the left side of Fig. 1. Four unit cells are depicted for better correspondence with the Fe_3Si lattice. The structural models of Fe_3Si (below, given as a reference) and $FeGe_2$ (above, our proposal) are drawn. The experimental micrographs are compared to the structural models, giving an illustration of our proposal of the $FeGe_2$ structure. On the other hand, the well-known structure of the Fe_3Si films is well reproduced, and so we can be sure that we described the $FeGe_2$ structure in a good approximation.

The verification of the proposed $FeGe_2$ structure (see Fig. 1) can be done using a computer simulation of the HAADF micrographs. We performed the simulations in the frozen phonon approximation using the parameters of the probe-C_s-corrected high-resolution (HR)-STEM (JEOL ARM200) operating at 200 kV. Simulations and experimental micrographs shown in Fig. 1 agree well, indicating that a proper structural model was found. The location of the 5 at. % Si detected by EDX spectroscopy is still unclear. The Si atoms probably are located on Ge sites. Besides, we found differently ordered regions of the Fe_3Si, the $B2$ order located near the interface and the DO_3 order in depth of the Fe_3Si film [41].

In Fig. 2, nanobeam diffraction patterns of the $FeGe_2$ thin film from [100]- and [110]-oriented samples are given. The patterns were fully indexed using the proposed $FeGe_2$ structure model and simulated in kinematical approximation. The results of the simulations given below in red color agree well with the experiments, further supporting our structural model.

In Fig. 3, the XRD curve (symmetrical $\omega/2\Theta$ scan, i.e., the $00L$ crystal truncation rod) together with the simulation of the diffraction curve of the $Fe_3Si/FeGe_2/Fe_3Si$ film stack in the vicinity of the GaAs(002) peak are shown. Here, the simulated diffraction curve agrees with the main features of the experimental diffraction curve, especially the $FeGe_2$ 001 and 003 maxima are visible, and the $FeGe_2$ 002 peak is shifted

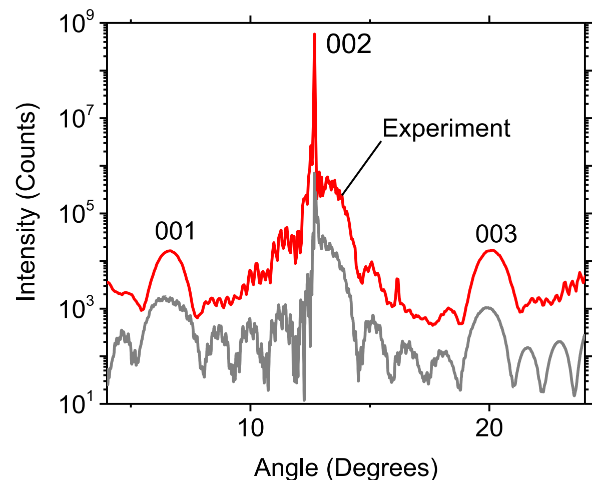

FIG. 3. Comparison of the measured XRD curve and the corresponding simulation (below) near GaAs(002) for the $Fe_3Si/FeGe_2/Fe_3Si$ film stack on GaAs(001), obtained using the structure shown in Fig. 1.

TABLE I. Experimental lattice parameters (determined by XRD) a of Fe_3Si, and $2a$ and c of $FeGe_2$ films grown on a GaAs(001) substrate in comparison with unstrained lattice parameters of Fe_3Si and $FeGe_2$ calculated by density functional theory for PBE and HSE functionals.

	Expt.	PBE	HSE
a (Fe_3Si)	0.5654 nm	0.561 nm	0.575 nm
$2a$ ($FeGe_2$)	0.5654 nm	0.572 nm	0.580 nm
c ($FeGe_2$)	0.5517 nm	0.544 nm	0.549 nm

with respect to GaAs 002. The XRD reciprocal space map of the nonsymmetric $20L$ crystal truncation rod is shown in the Supplemental Material [25]. All relevant diffraction maxima of the reciprocal space map are positioned on a vertical line perpendicular to the sample surface, i.e., the structures are elastically strained and no plastic relaxation occurs [42]. From XRD we deduce the lateral lattice parameter of the epitaxial layer stack $a = 0.5654$ nm $= 2 \times 0.2827$ nm and the strained vertical lattice parameter of the $FeGe_2$ thin film of $c = 0.5517$ nm (cf. Table I). A more careful analysis of the STEM HAADF micrographs allowed for a determination of the strained lattice plane distances of two types of sublayers in the $FeGe_2$ structure, viz., empty and filled ones. Empty layers and filled layers have distances of $c_1 = 0.266$ nm and and $c_2 = 0.282$ nm, respectively. Filling with Fe leads to an expansion of the distance of the corresponding layer. This fact points to the possibility of strain compensation between the two sublayers of the $FeGe_2$ lattice as a driving force for the formation of the ordered superlatticelike structure in the epitaxial layer stack [43]. On the other hand, the integral layer thickness $c_1 + c_2$ determined by STEM corresponds well to the strained c value determined by XRD for the $FeGe_2$ tetragonal lattice as a whole (see above). The theoretical values of the lattice parameters in Table I are given for unstrained lattices. In an epitaxial layer stack additional tetragonal deformation occurs [35,44].

Our results show that the ordering can be considered as a systematic arrangement of Fe atoms and vacancies in a CsCl-type FeGe lattice, where both atoms and vacancies are found on the Fe sites, and the number of Fe atoms is reduced by half in order to obtain the stoichiometry of $FeGe_2$. A random positioning of the Fe atoms would lead to a cubic lattice. But in our case we have the boundary condition at the $FeGe_2/Fe_3Si$ interface, where the in-plane lattice parameter of $FeGe_2$ is fixed to a value of 0.2827 nm. Let us take two CsCl-type unit cells to describe the $FeGe_2$ lattice as a result of the ordering of the Fe atoms and vacancies. Then, the diffraction intensity of the fundamental 002 reflection is proportional to $|f_{Fe} + 2f_{Ge}|^2$, where f_{Fe} and f_{Ge} are the atomic form factors of the Fe atom and the Ge atom, respectively. The intensity of the 001 superlattice reflection is

$$I(\vec{k}) \sim |\eta f_{Fe} - (1-\eta) f_{Fe}|^2, \tag{4}$$

because all other contributions vanish and only the ordered Fe atoms give a diffraction signal. From the comparison of the intensities of the layer reflections 001 (superlattice) and 002 (fundamental), we obtain $\eta = (0.805 \pm 0.02)$, i.e., the ordering is nearly complete. The film consists of an almost ideal $FeGe_2$ lattice. From the principle of minimum free energy the energy V lost by an atom moving from a disorder position to an order position can be calculated in the Gorsky-Bragg-Williams approximation [5,6]. This means in our case

$$V = kT \log[(1+\eta)/(1-\eta)]. \tag{5}$$

For an order parameter $\eta = 0.805$ and our annealing temperature of $T = 513$ K, we obtain $V = (0.042 \pm 0.02)$ eV per atom.

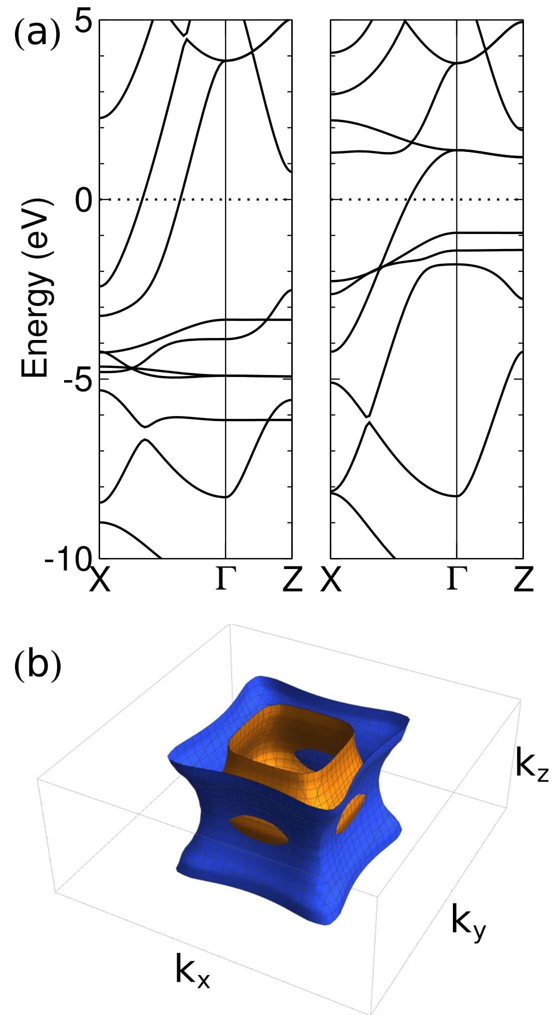

FIG. 4. (a) Band structure of $FeGe_2$ in the $P4mm$ structure calculated using DFT with the HSE screened hybrid functional. The left panel is the majority spin; the right panel is the minority spin. (b) Fermi surfaces for majority (dark, blue) and minority (bright, gold) spins. A second sheet in the majority spin channel is not shown.

Owing to the ordered structure of the $FeGe_2$ film with the extended Fe sheets we are expecting outstanding properties of this material. As a first step, using the structural data of the $FeGe_2$ obtained in the present Rapid Communication, we have calculated by DFT the band structure shown in Fig. 4(a). We can see that the Fermi surfaces in Fig. 4(b) consist of cylinders along the z axis, i.e., perpendicular to the Fe sheets. The electrical properties in the plane of the Fe sheets probably will differ considerably from those perpendicular to

the sheets. $FeGe_2$ belongs to a class of quasi-two-dimensional materials similar to MoS_2 [45]. Two-dimensional $FeGe_2$ can now be fabricated with a thickness down to 1 nm, and high-T_C superconductivity seems to be possible in such a structure [46–49]. Owing to the well-ordered Fe sheets, the concentration waves can be accompanied by spin-density waves.

Single-crystal Ge-rich films were successfully grown by solid-phase epitaxy on $Fe_3Si(001)$. Surprisingly, the structure of the films was not the expected diamond structure of Ge, but a well-oriented and layered tetragonal $FeGe_2$ $P4mm$ structure. A lattice misfit caused by interdiffusion of Si, Fe, and Ge leads to the formation of a different structure and ordering inside the film. We observe here one of the rare cases, where epitaxy is causing the formation of a distinct crystal structure differing from the equilibrium bulk structure, in particular, the strain-induced ordering of the $FeGe_2$ film with a periodicity along the direction perpendicular to the $FeGe_2/Fe_3Si$ interface.

The authors thank C. Herrmann for her support during the MBE growth, D. Steffen, M. Matzek, and S. Krauß for sample preparation, and U. Jahn for a critical reading of the manuscript and helpful discussion. This work was supported in part by the Office of Naval Research through the Naval Research Laboratory's Basic Research Program. Some computations were performed at the DoD Major Shared Resource Center at AFRL. We thank the Helmholtz-Zentrum Berlin (HZB) for providing beamtime at the BESSY-beamline U125/2 KMC with the endstation PHARAO.

[1] T. S. Kuan, T. F. Kuech, W. I. Wang, and E. L. Wilkie, Phys. Rev. Lett. **54**, 201 (1985).
[2] A. Ourmazd and J. C. Bean, Phys. Rev. Lett. **55**, 765 (1985).
[3] J. L. Martins and A. Zunger, Phys. Rev. Lett. **56**, 1400 (1986).
[4] A. A. Mbaye, L. G. Ferreira, and A. Zunger, Phys. Rev. Lett. **58**, 49 (1987).
[5] W. Gorsky, Z. Phys. **50**, 64 (1928).
[6] E. J. Willliams, Proc. R. Soc. London, Ser. A **152**, 231 (1935).
[7] A. G. Khachaturyan, Phys. Status Solidi B **60**, 9 (1973).
[8] A. G. Khachaturyan, *Theory of Structural Transformations in Solids* (Wiley, New York, 1983).
[9] A. V. Ruban and I. A. Abrikosov, Rep. Prog. Phys. **71**, 046501 (2008).
[10] I. A. Zhuravlev, J. M. An, and K. D. Belashchenko, Phys. Rev. B **90**, 214108 (2014).
[11] J. S. Wróbel, D. Nguyen-Manh, M. Y. Lavrentiev, M. Muzyk, and S. L. Dudarev, Phys. Rev. B **91**, 024108 (2015).
[12] B. P. Tinkham, B. Jenichen, V. M. Kaganer, R. Shayduk, W. Braun, and K. H. Ploog, J. Cryst. Growth **310**, 3416 (2008).
[13] B. Jenichen, V. M. Kaganer, R. Shayduk, W. Braun, and A. Trampert, Phys. Status Solidi A **206**, 1740 (2009).
[14] B. Jenichen, V. M. Kaganer, J. Herfort, D. K. Satapathy, H.-P. Schonherr, W. Braun, and K. H. Ploog, Phys. Rev. B **72**, 075329 (2005).
[15] S. Yamada, K. Tanikawa, M. Miyao, and K. Hamaya, Cryst. Growth Des. **12**, 4703 (2012).
[16] B. Jenichen, J. Herfort, U. Jahn, A. Trampert, and H. Riechert, Thin Solid Films **556**, 120 (2014).
[17] M. Kawano, M. Ikawa, K. Arima, S. Yamada, T. Kanashima, and K. Hamaya, J. Appl. Phys. **119**, 045302 (2016).
[18] S. Gaucher, B. Jenichen, J. Kalt, U. Jahn, A. Trampert, and J. Herfort, Appl. Phys. Lett. **110**, 102103 (2017).
[19] S. Sakai, M. Kawano, M. Ikawa, H. Sato, S. Yamada, and K. Hamaya, Semicond. Sci. Technol. **32**, 094005 (2017).
[20] M. Kawano, M. Ikawa, K. Santo, S. Sakai, H. Sato, S. Yamada, and K. Hamaya, Phys. Rev. Materials **1**, 034604 (2017).
[21] K. Hamaya, Y. Baba, G. Takemoto, K. Kasahara, S. Yamada, K. Sawano, and M. Miyao, J. Appl. Phys. **113**, 183713 (2013).
[22] K. Wu, U.S. Patent No. 6963121 (8 November 2005).
[23] S. Yuasa and D. D. Djayaprawira, J. Phys. D: Appl. Phys. **40**, R337 (2007).
[24] M. Oogane and S. Mizukami, Philos. Trans. R. Soc., A **369**, 3037 (2011).
[25] See Supplemental Material at http://link.aps.org/supplemental/10.1103/PhysRevMaterials.2.051402 for a more detailed description of the TEM and XRD experiments as well as the results of energy dispersive x-ray (EDX) spectroscopy, HAADF original data, and XRD reciprocal space mapping.
[26] P. Stadelmann, Electron Microscopy Simulation JEMS, http://www.jems-saas.ch/ (2016).
[27] CRYSTALMAKER, software for interactive crystal/molecular structures: modeling and diffraction by CRYSTALMAKER Software Limited, http://www.crystalmaker.com/ (2017).
[28] S. A. Stepanov, Collection of x-ray software, http://sergey.gmca.aps.anl.gov/ (1997).
[29] J. P. Perdew, K. Burke, and M. Ernzerhof, Phys. Rev. Lett. **77**, 3865 (1996).
[30] G. Kresse and J. Furthmuller, Phys. Rev. B **54**, 11169 (1996).
[31] G. Kresse and J. Furthmueller, Comput. Mater. Sci. **6**, 15 (1996).
[32] J. P. Perdew, M. Ernzerhof, and K. Burke, J. Chem. Phys. **105**, 9982 (1996).
[33] J. Heyd, G. E. Scuseria, and M. Ernzerhof, J. Chem. Phys. **118**, 8207 (2003).
[34] J. Herfort, A. Trampert, and K. H. Ploog, Int. J. Mater. Res. **97**, 1026 (2006).
[35] The Si content of 5 at. % can lead in principle to a lattice contraction of about 0.4%. We neglect this in the present Rapid Communication, because we do not know the position of the Si atoms in the lattice.
[36] R. Jaafar, D. Berling, D. Sébilleau, and G. Garreau, Phys. Rev. B **81**, 155423 (2010).
[37] N. S. Satyamurthy, R. J. Begum, C. S. Somanathan, and M. R. Murthy, Solid State Commun. **3**, 113 (1965).
[38] S. J. Pennycook and D. E. Jesson, Phys. Rev. Lett. **64**, 938 (1990).
[39] S. VanAert, K. J. Batenburg, M. D. Rossel, R. Erni, and G. VanTendeloo, Nature (London) **470**, 374 (2011).
[40] J.-M. Zuo, A. Shah, H. Kim, Y. Meng, W. Gao, and J.-L. Rouviére, Ultramicroscopy **136**, 50 (2014).
[41] M. Hashimoto, A. Trampert, J. Herfort, and K. H. Ploog, J. Vac. Sci. Technol. B **25**, 1453 (2007).
[42] H. Heinke, M. O. Möller, D. Hommel, and G. Landwehr, J. Cryst. Growth **135**, 41 (1994).
[43] DFT yielded the lattice parameters of, first, a hypothetical primitive Ge lattice, $a = 0.268$ nm ($a = 0.272$ nm), and, second, a hypothetical CsCl-type GeFe lattice, $a = 0.288$ nm ($a = 0.290$ nm), correspondingly for the HSE (PBE) functional. The

halved lattice parameter $a/2$ of Fe_3Si of 0.2827 nm lies between those values of the DFT calculations for the hypothetical primitive and the CsCl-type lattices, so that a strain compensation between the two parts of the $FeGe_2$ lattice seems possible.

[44] J. Hornstra and W. J. Bartels, J. Cryst. Growth **44**, 513 (1978).

[45] W. Rotjanapittayakul, W. Pijitrojana, T. Archer, S. Sanvito, and J. Prasongkit, Sci. Rep. **8**, 4779 (2018).

[46] G. R. Stewart, Rev. Mod. Phys. **83**, 1589 (2011).

[47] W. Miiller, J. M. Tomczak, J. W. Simonson, G. Smith, G. Kotliar, and M. C. Aronson, J. Phys.: Condens. Matter **27**, 175601 (2015).

[48] J.-F. Ge, Z.-L. Liu, C. Liu, C.-L. Gao, D. Qian, Q.-K. Xue, Y. Liu, and J.-F. Jia, Nat. Mater. **14**, 285 (2015).

[49] Y. Zhou, L. Miao, P. Wang, F. F. Zhu, W. X. Jiang, S. W. Jiang, Y. Zhang, B. Lei, X. H. Chen, H. F. Ding, H. Zheng, W. T. Zhang, J. F. Jia, D. Qian, and D. Wu, Phys. Rev. Lett. **120**, 097001 (2018).